

Available online at [www.sciencedirect.com](http://www.sciencedirect.com)

Chemical Engineering Research and Design

journal homepage: [www.elsevier.com/locate/cherd](http://www.elsevier.com/locate/cherd)

IChemE



# Performance analysis of methanol steam micro-reformers for enhanced hydrogen production using CFD

Debanik Bose, Indradev Kumar, Abhiram Hens\*

Department of Chemical Engineering, National Institute of Technology Durgapur, Durgapur 713209, India

## ARTICLE INFO

### Article history:

Received 23 March 2023

Received in revised form 7 June 2023

Accepted 25 June 2023

Available online 29 June 2023

### Keywords:

Steam reforming

Hydrogen production

CFD

Spiral reformer

## ABSTRACT

Present study shows the performance analysis of methanol steam reforming considering different miniature-scale reformer geometries. Three different types of 3D models of steam reformers have been considered: straight annular, spiral, and serpentine-type reactors. Each reformer is packed with a copper-based catalyst to enhance the reaction between steam and methanol. Methanol steam reforming is an endothermic reaction with a two-step mechanism, whose reaction kinetic models were mathematically implemented. The study shows different hydrodynamic aspects of the flow fields through the catalyst bed, the conversion of methanol, and production of hydrogen for each type of reactors. Simulations were carried out at different temperatures and inlet velocities to study the methanol conversion and identify the most optimized reformer design. It was found that in the spiral and serpentine-type reformer, the methanol conversion was more due to the bending in the tubular reactor, which disturbs the flow field with an enhancement of mixing, causing more conversion. Spiral reformer exhibited conversion up to 91.16% at 650 K and producing 0.15 mass fraction of hydrogen, which was found to be 3% more than the conversion achieved in serpentine type and almost 8% more than the straight annular type geometry when the inlet velocity was kept at 0.1 m/s for all the cases.

© 2023 Institution of Chemical Engineers. Published by Elsevier Ltd. All rights reserved.

## 1. Introduction

Hydrogen is available in large quantities on earth in different forms. Use of hydrogen as fuel can solve lots of problems related to carbon dioxide emissions. Hydrogen is also known for its characteristics such as renewable and non-polluting (due to the absence of carbon) nature in comparison to other fuels (Luo et al. 2019; Niu et al. 2016; Sun et al., 2016). It is considered as the cleanest and the greenest fuel available to us and called a “zero-emission or emission-free fuel.” When diesel is replaced by hydrogen by 2% in terms of energy share, approximately 2.5% of CO<sub>2</sub> emission is reduced (Chiriac et al. 2015). Only a few methods or reactions are commercially available for hydrogen production or

extraction, and one of them is the steam reforming reaction. Other methods like auto thermal reforming, partial oxidation, electrolysis, and membrane-based technology are also known for hydrogen production at different scales. Fuel cells (FC) are known as an alternative source of energy (hydrogen) due to high energy efficiency and environmental friendly properties (Hall, 1987; Kreuer, 2001).

Hydrogen can be used in internal combustion engines because it can improve the performance of engine and reduce emissions. Application of hydrogen can improve the combustion stability and extend the lean burn limit to the methanol-fed DISI (Direct Injection Spark Ignition) engine with an approximately 2.95 excess air ratio (Gong et al. 2020; Gong et al. 2020). By using flue gas temperatures up to 600 K, it was explained that methanol is a better fuel for reforming than other alternative fuels such as ethanol, glycerol, propane and methane, providing maximum heat recovery (Pashchenko, 2020). In comparison to other endothermic

\* Corresponding author.

E-mail address: [abhiram.hens@che.nitdgp.ac.in](mailto:abhiram.hens@che.nitdgp.ac.in) (A. Hens).<https://doi.org/10.1016/j.cherd.2023.06.051>

0263-8762/© 2023 Institution of Chemical Engineers. Published by Elsevier Ltd. All rights reserved.

reforming reactions such as pyrolysis and dry-reforming, the yield of hydrogen in the case of methanol steam reforming (MSR) is higher and it consumes less energy (Duc-Khanh and Verhelst (2019)). Methanol is suitable for IC engines because it requires low temperatures (200–350 °C) to undergo the endothermic reforming reaction (Nehe et al. (2015)). Cu-based methanol steam reforming catalysts are commonly used in catalytic conversion processes (Davda et al. 2003; Duc-Khanh and Verhelst (2019)). The most commonly used catalyst for MSR, are ZnO/CuO/Al<sub>2</sub>O<sub>3</sub> particles (Peppley et al. 1999). Catalysts can be packed in tubes to form a fixed-bed reactor or coated on the surface to form a fixed-bed reactor plate (Chen et al. 2011). Reactor geometry, steam to carbon ratio, reaction temperature, and flow patterns within the reactor are all essential factors that affect the performance of the reformer. In the reforming process, heat transfer in the reformer also plays an important role (Iulianelli et al. 2014; Meille, 2021) because heat must be supplied as an external heat source to carry out the reaction. Methanol-reforming is also considered as thermochemical waste-heat recuperation based method which is a promising technology for recovering waste heat that includes methanol from industrial processes and converting it into usable energy. This technology involves the use of a thermochemical cycle to produce hydrogen from steam and other sources, such as biomass or natural gas. One of the main advantages of this technology is that the synthetic fuel produced after reforming contains a high percentage of hydrogen, usually more than 50% (Pashchenko, 2021). This hydrogen can be used in a variety of applications, including fuel cells, transportation, and energy storage.

Many researchers investigated the MSR based hydrogen production process to increase its efficiency. For example, a computation study by Srivastava et al. (Srivastava et al., 2022), showed the use of heat extracted from the exhaust gas during the process of methanol-steam reforming. The study emphasized the effect of heat transfer in their model by adding straight fins and curved fins to enhance heat conduction. The heat supply was taken from the exhaust gas which flows surrounding the reformer channel. Another study by Perng et al. (Perng et al., 2017) demonstrated the effect of a diffuser in the reformer for the enhancement of the performance of the reforming reaction, by changing the angle of diffuser. Zhang et al. (Zhang et al. 2017) evaluated the performance of cross U-type and parallel U-type micro-reformers to produce a high yield of hydrogen. This was done both computationally and experimentally. A three dimensional analysis was done by Hsueh et al. (Hsueh et al. 2011) where a plate type methanol steam micro-reformer which was coupled with catalytic combustion of methanol was developed. The work showed the optimization of the reforming reaction using a serpentine flow field. The configuration improved the thermal management by utilizing the heat obtained from the exothermic combustion process in the ongoing MSR (endothermic) chamber. Gurau et al. (Gurau et al., 2020) reported an efficient design for hydrogen production in an on-board fuel cell using numerical simulations. Two operating regimes of fuel processor were considered, which resulted high methanol conversion and hydrogen production for a small reformer size. The objective of the study was also to verify that the outlet gas composition can be tolerated by phosphoric acid-doped high temperature proton exchange membrane fuel cell. Chein et al. (Chein et al. 2012) reported the effect of baffles inside an integrated

reformer-combustor, where the performance of reforming reaction was studied varying the number baffle plates and their angles. The baffle plates enhance the heat transfer due to the flow disturbance created inside the catalyst bed. It also resulted in an increase in pressure drop. Both experimental and numerical investigation of a glass-made methanol steam micro-reformer-combustor unit was performed by Kim (Kim, 2009) which demonstrated a good methanol conversion. Another study on integrated reformer-combustor performed by Tadbir et al. (Tadbir and Akbari, 2011), investigated the effect of catalyst thickness, gas hourly space velocities, reactor geometry, separating substrate properties, and inlet composition of the steam reformer. For generating 100 W power fuel cell by hydrogen, a micro methanol steam reformer was modelled and simulated by Vadlamudi et al. (Vadlamudi and Palanki, 2011). A multichannel methanol steam reformer for syngas production was incorporated by Zhuang et al. (Zhuang et al. 2020), which used the triple rate kinetic model of methanol steam reforming. The results were mainly based on the effect of steam to carbon molar ratio, weight hourly space velocity, operating temperature and catalyst layer thickness. Most of these studies attempted to increase the hydrogen production rate through MSR by changing various parameters. However, changing the overall geometry of the reformer, especially, the use of spiral and serpentine geometry has not been addressed so far.

This present work numerically investigates the reformer performances with respect to hydrogen production by considering different geometries of MSR-based micro-reactors. The conventional design of the reformer (i.e., straight annular type) was analysed with a Cu-based catalyst-packed bed of a certain length, and heat is applied directly on the wall as a temperature source. Two more types of reactor models were investigated considering serpentine and spiral geometry. CFD analysis of these reformers was done at three different temperatures; 550, 600, and 650 K and at different inlet gas velocities; 0.1, 0.15, 0.2, 0.25, and 0.3 m/s. A comparison of the results of these types of reformers were presented and analysed.

## 2. Methodology

In the present study, three-dimensional numerical models were formulated and computational fluid dynamics (CFD) based simulations were performed. All gases were assumed to act as an ideal gas, and the flow was considered to be turbulent and incompressible. A steady-state pressure driven flow through the tubular channel was considered. The influence of any external body force and gravity were ignored. No thermal radiation within the gas phase was considered. The catalyst bed was assumed to be porous and isotropic with uniform physio-chemical properties throughout the bed length. Temporal decay of the catalyst was also neglected. The reaction would only take place in the catalytic porous zone. All the simulations were performed using the solver of ANSYS Fluent 2022R2 (Fluent and ANSYS (2013)).

### 2.1. Geometry

Three different types of geometry were designed for the study of reactor performance. These reactors are basically tubular channels with uniform cross sections at a miniature scale, through which the reactant gases flow. In the present study, the inner metal surface of the reactor channel and the

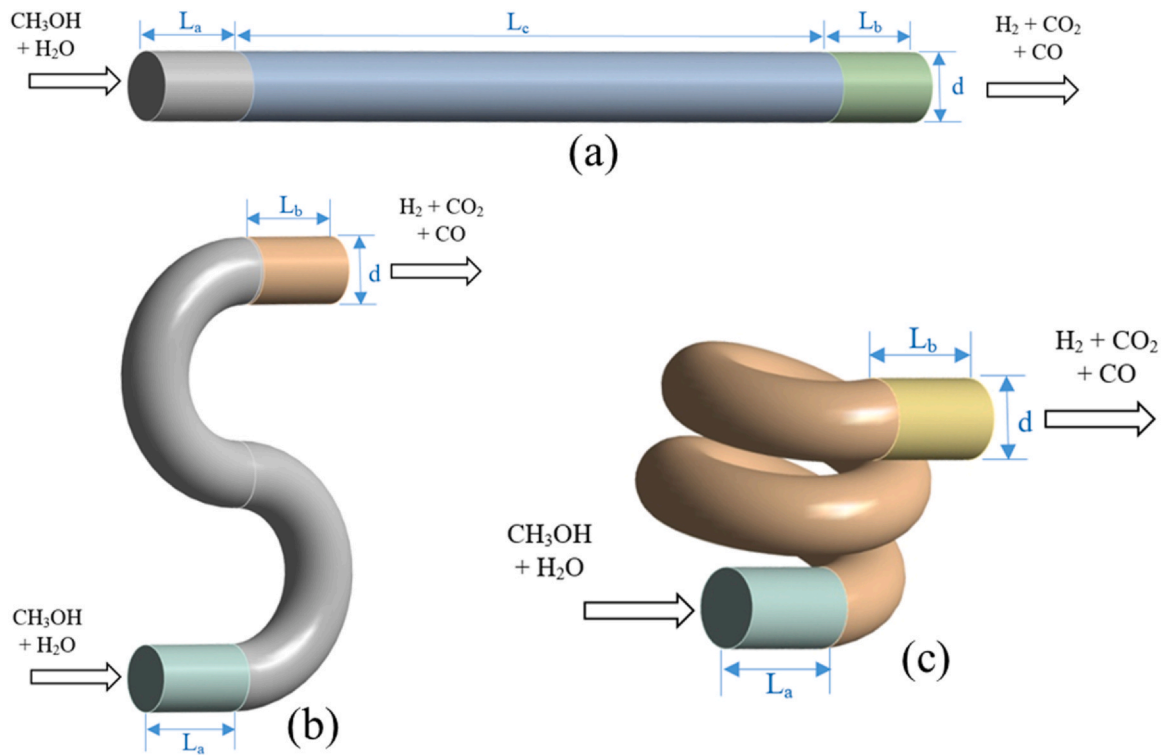


Fig. 1 – (a) Straight annular; (b) Serpentine; (c) Spiral type reformer.

flow domain were considered for carrying out the simulation of the reforming reaction which takes heat from the wall surface. The conceptual design for the normal straight annular reactor was based on a reported study of Srivastava et al. (Srivastava et al. 2022). The spiral and serpentine reactors, which were considered in the present study are shown in Fig. 1. All three reactors were packed with Cu-based catalyst particles, and the diameter ( $d$ ) of the reactor was considered to be 20 mm for comparing the efficiency of different geometries. The reactants will flow through the inlet section ( $L_a=30$  mm) which is the distance between the inlet and the catalyst bed. A flow path of similar distance ( $L_b=30$  mm) was kept in between the catalyst bed and the outlet. The length of the catalyst bed ( $L_c$ ) was considered as 200 mm in each case of the reactor. Thus, the total length and volume becomes same for all the geometries. The length provided before the reactants enter the catalyst zone is for preheating the gases. The straight annular reactor was simulated first, following the serpentine and spiral reactors.

It is important to mention here that the initial 30 mm length, that we considered is consistent with the study of Srivastava et al. (Srivastava et al. 2022). The choice of a 420 K inlet gas temperature was also influenced by this research, which demonstrated its effectiveness in promoting the reforming reaction. The initial free flow zone serves not only for pre-heating but also for distinguishing the hydrodynamics between the catalyst-packed and free-flowing regions. This approach facilitates logical and comprehensible analysis of contour diagrams. For the same reason, the 30 mm length at the outlet was also considered.

## 2.2. Governing equations

For the CFD analysis, the governing equations were mainly based on conservation equations of mass, momentum and energy. The equations are shown as follows:

Continuity equation:

$$\rho \left( \frac{\partial u}{\partial x} + \frac{\partial v}{\partial y} + \frac{\partial w}{\partial z} \right) = 0 \quad (1)$$

Here,  $u$ ,  $v$ , and  $w$  are the velocity components in  $x$ ,  $y$ , and  $z$  directions respectively.

Navier-Stokes equations:

X-momentum equation:

$$\varepsilon \rho \left( u \frac{\partial u}{\partial x} + v \frac{\partial u}{\partial y} + w \frac{\partial u}{\partial z} \right) = -\varepsilon \frac{\partial p}{\partial x} + \varepsilon \mu \left( \frac{\partial^2 u}{\partial x^2} + \frac{\partial^2 u}{\partial y^2} + \frac{\partial^2 u}{\partial z^2} \right) + S_u \quad (2)$$

Y-momentum equation:

$$\varepsilon \rho \left( u \frac{\partial v}{\partial x} + v \frac{\partial v}{\partial y} + w \frac{\partial v}{\partial z} \right) = -\varepsilon \frac{\partial p}{\partial y} + \varepsilon \mu \left( \frac{\partial^2 v}{\partial x^2} + \frac{\partial^2 v}{\partial y^2} + \frac{\partial^2 v}{\partial z^2} \right) + S_v \quad (3)$$

Z-momentum equation:

$$\varepsilon \rho \left( u \frac{\partial w}{\partial x} + v \frac{\partial w}{\partial y} + w \frac{\partial w}{\partial z} \right) = -\varepsilon \frac{\partial p}{\partial z} + \varepsilon \mu \left( \frac{\partial^2 w}{\partial x^2} + \frac{\partial^2 w}{\partial y^2} + \frac{\partial^2 w}{\partial z^2} \right) + S_w \quad (4)$$

In the above equations,  $S_u$ ,  $S_v$ , and  $S_w$  denote the momentum source terms of the reactant gas flow in the porous zone of catalyst bed. The source terms;  $S_u$ ,  $S_v$ , and  $S_w$  only exist when there is a flow through the porous region. Hence their value will be zero for free-flowing region. These terms produced due to porous catalyst and can be expressed by the equation:

$$S_u = -\frac{\mu u}{k} - \frac{\beta u \rho}{2} \sqrt{u^2 + v^2 + w^2} \quad (5)$$

$$S_v = -\frac{\mu v}{k} - \frac{\beta v \rho}{2} \sqrt{u^2 + v^2 + w^2} \quad (6)$$

$$S_w = -\frac{\mu w}{k} - \frac{\beta w \rho}{2} \sqrt{u^2 + v^2 + w^2} \quad (7)$$

**Table 1 – Physical properties of the catalyst.**

Property	Value	Reference
Catalyst density (kg/m <sup>3</sup> )	1480	(Karim et al., 2005)
Catalyst thermal conductivity (W/mK), $\lambda_c$	1	(Karim et al. 2005)
Catalyst bed porosity, $\varepsilon$	0.5	(Perng et al. 2017)
Catalyst bed permeability (m <sup>2</sup> ), $k$	$2.379 \times 10^{-12}$	(Karim et al., 2005)

The source terms;  $S_u$ ,  $S_v$ , and  $S_w$  in the above equations, can also be expressed as overall momentum source term  $S_m$ , as the following equation:

$$S_m = -\frac{\mu}{\rho_f k} \vec{\nabla} - \frac{\beta \vec{\nabla}}{2} |\vec{\nabla}| \quad (8)$$

Where,  $k$  represents permeability, and  $\beta$  represents inertial loss coefficient along each direction in the porous medium of catalyst bed which causes a pressure drop. By using Ergun equations (Burke and Plummer, 1928), these terms are obtained and are shown as following expression:

$$k = \frac{d_p^2 \varepsilon^3}{150(1 - \varepsilon)^2} \quad (9)$$

$$\beta = \frac{3.5(1 - \varepsilon)}{d_p \varepsilon^3} \quad (10)$$

Where,  $d_p$  denotes particle diameter of each catalyst particles.

In the momentum equations,  $\varepsilon$  denotes the porosity of the catalyst medium (volume of fluid in porous region/ total volume of catalyst) and  $\mu_{mix}$  is the viscosity of the gas mixture (White, 1991) which is given by Eq. (11):

$$\mu_{mix} = \sum_{i=1}^5 \frac{M_i \mu_i}{M_j \phi_{ij}} \quad (11)$$

and  $\phi_{ij}$  is expressed as Eq. (12):

$$\phi_{ij} = \sum_i \frac{\left[ 1 + \left( \frac{\mu_i}{\mu_j} \right)^{\frac{1}{2}} \left( \frac{M_{w,j}}{M_{w,i}} \right)^{\frac{1}{4}} \right]^2}{\left[ 8 \left( 1 + \frac{M_{w,i}}{M_{w,j}} \right) \right]^{\frac{1}{2}}} \quad (12)$$

$\phi_{ij}$  in Eq. 12 is a normalization factor in Wilke's mixture rule, accounting for component fractions and their influence on the overall viscosity, ensuring an appropriate scaling of the weighted average viscosity in the gas mixture calculation (Mathur and Saxena, 1965).

Here,  $M_{wi}$  is the the molecular weight of the  $i^{\text{th}}$  species in kg/mol. Species transport equation is represented as Eq. (13):

$$\varepsilon \left( u \frac{\partial m_i}{\partial x} + v \frac{\partial m_i}{\partial y} + w \frac{\partial m_i}{\partial z} \right) = D_{eff} \left( \frac{\partial^2 m_i}{\partial x^2} + v \frac{\partial^2 m_i}{\partial y^2} + w \frac{\partial^2 m_i}{\partial z^2} \right) + \varepsilon \sum_{r=1}^N M_{wi} R_{ir} \quad (13)$$

In the above equation, mass fraction of the  $i^{\text{th}}$  species is denoted by  $m_i$ , where the  $i^{\text{th}}$  species stands for CH<sub>3</sub>OH, H<sub>2</sub>O, H<sub>2</sub>, CO<sub>2</sub>, and CO. These equations can also be expressed in terms of species concentration equation:

$$\varepsilon (\vec{\nabla} \cdot \nabla) C_i = D_{eff} \nabla^2 C_i + \varepsilon \sum_{r=1}^N M_{wi} R_{ir} \quad (14)$$

Where,  $C_i$  is the  $i^{\text{th}}$  species concentration,  $R_{ir}$  is the Arrhenius rate of reaction of  $i^{\text{th}}$  species of  $r^{\text{th}}$  reaction in mol/m<sup>3</sup>-s. Again, the last term in the species transport equation is the source term which is due to the reactions in presence of

catalyst material.  $D_{eff}$  denotes the effective diffusion coefficient given by Stefan-Maxwell equations (White, 1991). Due to the presence of catalyst, the effective diffusion coefficient is influenced by the porosity ( $\varepsilon$ ) and it is expressed by Eq. (15):

$$D_{eff} = D_k \varepsilon^r \quad (15)$$

Where,  $D_k$  denotes mass diffusion coefficient in absence of porosity.

The expression of energy equation is given by Eq. (16):

$$(\rho_f C_p) (\vec{\nabla} \cdot \nabla) T = \lambda_{eff} \nabla^2 T + \varepsilon S_t \quad (16)$$

Where, effective thermal conductivity of the porous catalyst medium is denoted by  $\lambda_{eff}$ , and this can be expressed by Eq. (17):

$$\lambda_{eff} = \varepsilon \lambda_f + (1 - \varepsilon) \lambda_c \quad (17)$$

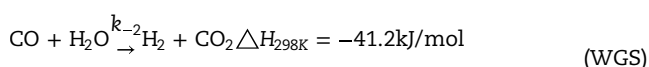
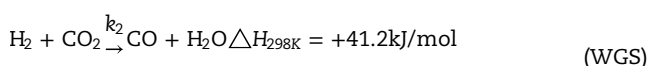
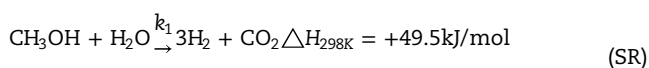
Here,  $\lambda_f$  is the fluid thermal conductivity and  $\lambda_c$  is the solid thermal conductivity in the porous zone and  $\lambda_{eff}$  is the effective thermal conductivity. Since, reaction occurs in the porous zone, the source term is present in the equation, which can be expressed as Eq. (18):

$$S_t = - \sum_{i=1}^N \left( \frac{h_i^0}{M_{wi}} + \int_{T_{ref}}^T C_{pi} dT \right) (R_{ir}) \quad (18)$$

Where  $N$  is the number of chemical species taking part in chemical reaction,  $h_i^0$  is the enthalpy of  $i^{\text{th}}$  species in kJ/mol,  $C_{pi}$  is the specific heat capacity of the  $i^{\text{th}}$  species in kJ/kg-K, and Table 1 shows the physical properties of the catalyst.

### 2.3. Chemical kinetics

Methanol-steam reforming is an endothermic reaction with a two-step mechanism. It consists of a non-reversible steam reforming (SR) (first step), and a reversible water gas shift reaction (WGS) (second step), whose reaction kinetic models are mathematically implemented and the values are shown in Table 2. SR and WGS reactions are mainly considered in the present study.



The importance of the water gas shift reaction in reforming lies in its ability to enhance the hydrogen production and remove excess carbon monoxide.

The evaluation of the rate of above reactions are done by using Arrhenius model (Agrell et al. 2002; Fukahori et al. 2008). The rate of SR and WGS reactions are expressed as (19) and (20);



**Table 2 – Chemical Kinetics parameters.**

Parameter	Value	Reference
Pre-exponential factor for SR ( $s^{-1}$ ), $k_1$	$8 \times 10^8$	(Agrell et al. 2002)(Fukahori et al. 2008)
Pre-exponential factor for forward WGS ( $m^3/mol\ s$ ), $k_2$	$4 \times 10^8$	(Agrell et al. 2002)(Fukahori et al. 2008)
Pre-exponential factor for backward WGS ( $m^3/mol\ s$ ), $k_{-2}$	$4 \times 10^8$	(Agrell et al. 2002)(Fukahori et al. 2008)
Activation energy for SR ( $J/mol$ ), $E_{a1}$	$7 \times 10^7$	(Agrell et al. 2002)(Fukahori et al. 2008)
Activation energy for forward WGS ( $J/mol$ ), $E_{a2}$	$1 \times 10^8$	(Agrell et al. 2002)(Fukahori et al. 2008)
Activation energy for backward WGS ( $J/mol$ ), $E_{a-2}$	$1 \times 10^8$	(Agrell et al. 2002)(Fukahori et al. 2008)

$$R_{SR} = k_1 C_{CH_3OH}^{0.6} C_{H_2O}^{0.4} \exp\left(-\frac{E_{a1}}{RT}\right) \quad (19)$$

$$R_{WGS} = k_2 C_{CO_2} C_{H_2} \exp\left(-\frac{E_{a2}}{RT}\right) - k_{-2} C_{CO} C_{H_2O} \exp\left(-\frac{E_{a-2}}{RT}\right) \quad (20)$$

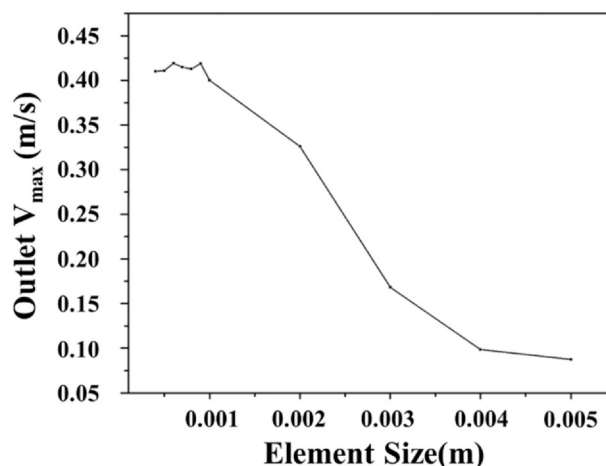
Here,  $R$  is the universal gas constant,  $k$  is the pre-exponential factor, and  $E_a$  is the activation energy.

#### 2.4. Boundary conditions

The governing equations were discretised using the finite volume method (FVM). Pressure-based steady-state solver was used to perform the numerical simulations. For reactions, species transport models were chosen, with finite rate kinetic model or no turbulence chemistry interaction (TCI) model. SST  $k$ - $\omega$  turbulent viscous model was used for the straight annular, spiral and serpentine reactor, since some turbulence or disturbance is supposed to generate in the flow regime due to the curved tubular channel. The velocity, temperature, species concentration and species flux at the interface between the free flow region and catalyst bed domain are considered to be continuous. Velocity-inlet and pressure outlet type of boundary conditions were employed. For pressure-velocity coupling, SIMPLE-C scheme was utilized (Taylor et al. (2007)) and discretization of the pressure term was done by PRESTO! (PREssure STaggering Option) scheme which was recommended for temperature-dependent thermophysical properties and flows involving porous media (Canonsburg and Technology Drive (2012)). Momentum, species, and energy equations were discretised by second upwind scheme. As convergence criteria, all the residual values are kept less than  $10^{-6}$ . Residual values are set to quantify errors in CFD simulations in each step. These values represent the difference of the parameters between two consecutive steps of iterations during the numerical solution of the governing equations. By setting a target residual for each parameter, users define the desired level of convergence. The solver monitors and compares residuals during iterations, and it will stop when the values fall below their residual limit.

No-slip boundary conditions were considered at the walls. Mass diffusion coefficient  $D_k$  was taken as  $6.8 \times 10^{-5} m^2/s$  (Karim et al., 2005). In the present study, the reactors are simulated at three different temperatures: 550 K, 600 K, and 650 K. Selection of this temperature range is purely based on the application in automobile engines, where the exhaust gas is generally available at around 600 K, which acts as a heat source for the reforming reaction.

At inlet, the reactant gases are preheated up to 420 K, and the reactor models were solved at different inlet velocities: 0.1 m/s, 0.15 m/s, 0.2 m/s, 0.25 m/s, and 0.3 m/s with an S/C

**Fig. 2 – Grid independence test.**

(steam to carbon) ratio of 1.1 for each case. At the outlet 0-gauge pressure was maintained.

A distinct cell zone was designated to set the porosity of the catalyst bed, called the "catalyst section" located in the middle section of all the geometries, as shown in Fig. 1. This cell zone was specified as a porous zone, which allowed us to model the porosity and other properties of the catalyst-packed bed. It is important to mention that in the present study, the porosity and permeability of the packed catalyst bed were considered neglecting the porosity inside the particles.

The grid-independence study (Fig. 2) was done on the straight annular channel, where the maximum velocity ( $V_{max}$ ) at the outlet was plotted against the size of the volume elements and it was noted that after reducing the element size lower than 0.001 m, the variation in the maximum velocity was not significant. So this element size was considered as the optimum one for the present study.

### 3. Results and discussion

The present study was started by validating the work of Srivastava et al. (Srivastava et al. 2022), where the simulation of methanol steam micro-reformer was shown. It was a straight annular geometry where the reformer reaction occurs in the inner cylinder taking heat energy from the hot exhaust gas flowing through the outer annular region. The present work does not consider the outer annular chamber and the temperature was specified directly on the wall surface of the reformer. The major objective was to analyse the effect of different geometries on the rate of hydrogen production. The straight annular reactor geometry was considered as a base case for comparing the performance of other reactor geometries. All the input parameters were kept same as Srivastava et al. Inlet velocity and wall temperature

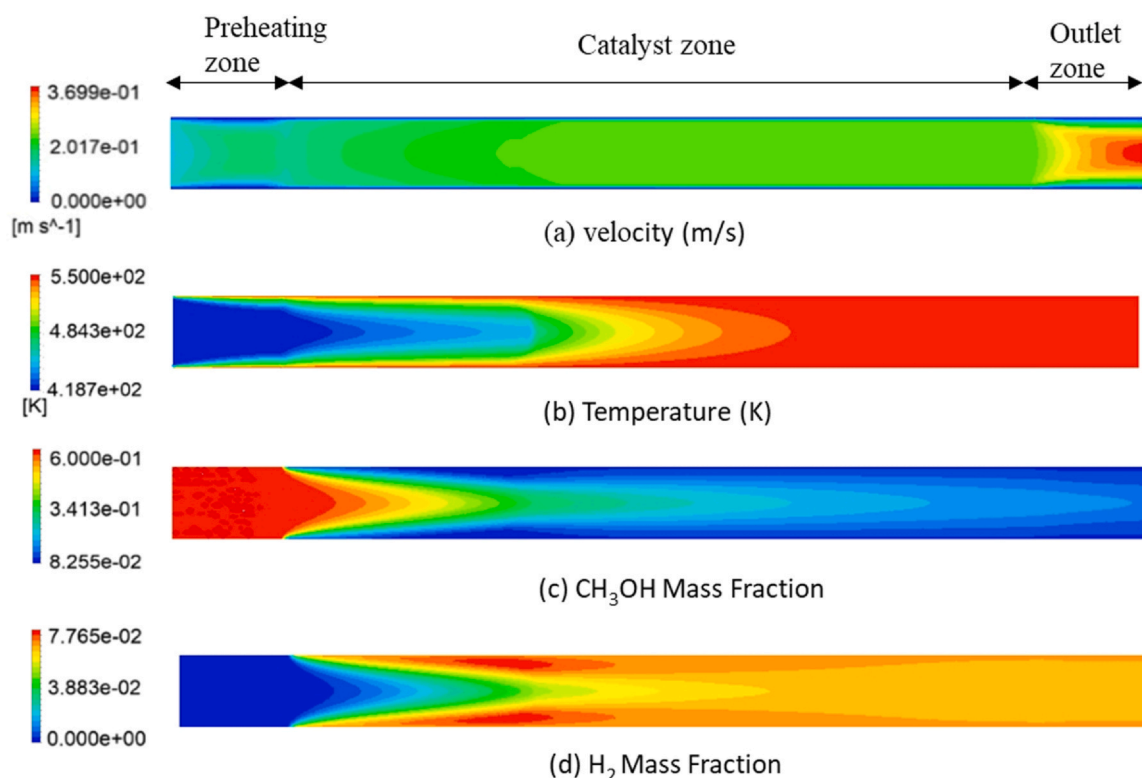


**Fig. 3 – Contour of (a) velocity, (b) temperature and species distribution for (c) methanol and (d) hydrogen along a cross-sectional plane of straight annular reformer.**

were considered as 0.1 m/s and 550 K respectively. S/C ratio was kept at 1.1 and reactants were pre heated to 420 K. The methanol conversion and the hydrogen production were compared with the results of Srivastava et al. and the results were found to be similar as show results in Fig. S1 (Supplementary Information). Keeping the parameters same, other geometries (i.e., spiral and serpentine reformers) were analysed for hydrogen production. The contour of velocity, temperature, methanol mass fraction and hydrogen mass fraction distribution of straight annular geometry was investigated at 0.1 m/s and 550 K wall temperature and are shown in Fig. 3.

### 3.1. Straight annular type reformer

In Fig. 3(a) the velocity contour was shown, where it was observed that, at the boundary of the annular channel the velocity was very minimum, and there was a little rise in velocity in the catalyst zone, and when the fluid leaved the packed bed, the velocity was abruptly increased. The temperature contour was shown in Fig. 3(b). It was observed that at the inlet section temperature was less because the pre-heating temperature was less than the reactor wall temperature. The temperature gradually increased after entering the catalyst zone due to the reduced velocity at the catalyst bed. The methanol mass fraction, shown in Fig. 3(c), was found to decrease gradually through the catalyst zone where the reaction was taking place and it was very less at the periphery of the reactor, indicating higher rate of reaction near the hot boundary. The hydrogen mass fraction contour, shown in Fig. 3(d), reveals that the hydrogen formation and accumulation was more at the periphery of the middle portion of catalyst zone, than at the outlet of the reformer. From the contours of the species, it was clear that methanol was

gradually decreasing, and hydrogen was increasing through the catalyst bed. The area average of methanol and hydrogen mass fraction at the outlet were found to be 0.151 and 0.069 respectively. The methanol conversion was calculated and found to be 74.83%. Velocity at the outlet was almost reaching up to 0.4 m/s which was 4 times more than the inlet velocity. The average temperature at the outlet was around 549 K.

### 3.2. Serpentine type reformer

In the case of serpentine type of reformer, the similar contour diagrams (at 550 K wall temperature and 0.1 m/s inlet gas velocity) have been generated and shown in Fig. 3. In the velocity contour, it was observed that at the bends in the catalyst zone of the reformer, the velocity was increased at the inner edge, whereas, on the opposite edge it was less, as shown in Fig. 4(a). And this distribution continues in the upper half of the reformer. The velocity was increased when the fluid leaved the catalyst zone and at the boundary of the reformer it was very less. The temperature distribution was observed to be similar to the straight annular type, however, it follows the bended path of the reformer, as shown in Fig. 4(b). The mass fraction of methanol and hydrogen gradually decreases and increases respectively, and at the boundary of the reformer methanol mass fraction was found to be less, as shown in Fig. 4(c). The hydrogen mass fraction was found to increase along the flow path as shown in Fig. 4(d). The methanol conversion and area average mass fraction of  $H_2$  at the outlet were found to be 79.85% and 0.083 respectively. The average velocity at outlet was 0.23 m/s, which was not so much increased as compared to the straight annular type indicating more residence time and better conversion in the serpentine geometry.

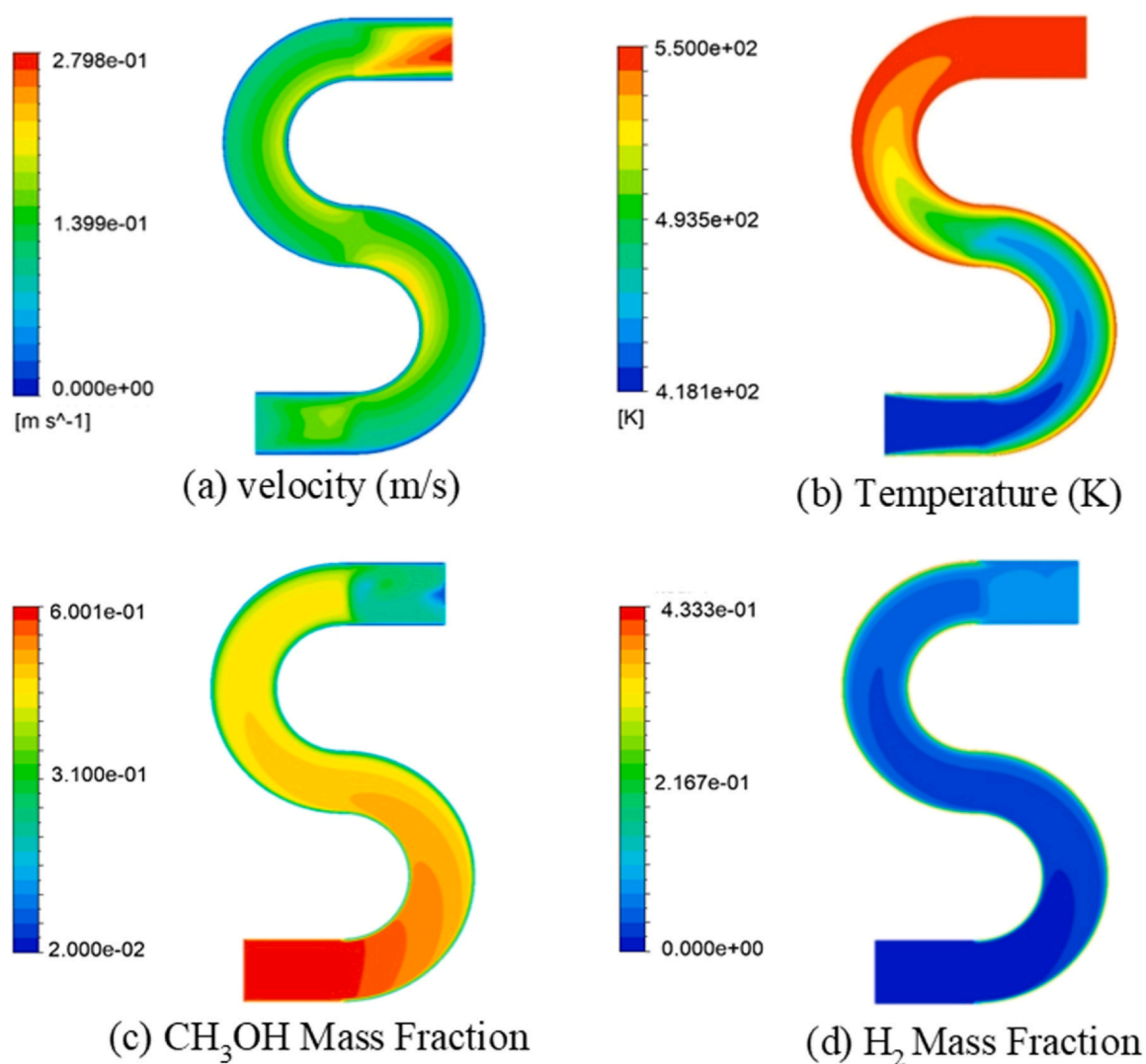


Fig. 4 – Contour of (a) velocity, (b) temperature and (c) & (d) species distribution along a cross-sectional plane of the serpentine reformer.

### 3.3. Spiral type reformer

The spiral reformer geometry is not linear along any of the axis in 3-dimensional space, hence, at every interval of 25 mm along the catalyst bed, the cross-sectional planes were taken to study the contour of the parameters, as shown in Fig. 5. The contours were generated at 550 K wall temperature and 0.1 m/s inlet velocity. It was observed from the temperature distribution, as shown in Fig. 5(a), that at the entry of the catalyst zone, the temperature was 420 K (pre-heating temperature) and the heat transfer in the catalyst bed region was observed along the curved channel. The velocity distribution, as shown in Fig. 5(b), depicts that the velocity was high at the inner peripheral region where, the gas mixture had to cover less distance comparative to the opposite region. Here also the velocity was minimum at the boundary of the reformer. The region inside the spiral reformer, where the temperature was more and velocity was less, it was observed that methanol mass fraction reduced due to receiving enough heat and sufficient reaction time for conversion. It was also observed that the hydrogen mass fraction gained in those regions (Fig. 5(c) and (d)). At the outlet, the average velocity was found to be 0.11 m/s and average temperature was 548 K. The conversion was found to

be maximum in this spiral geometry of the reformer, which was 82.67%, and area average of H<sub>2</sub> mass fraction gained at the outlet 0.098.

### 3.4. Comparative analysis

A comparison between the three types of reformers had been done to study the reaction performance in terms of methanol conversion and hydrogen production at different wall temperatures and gas inlet velocities. As shown in Fig. 6(a), methanol conversions were plotted against the wall temperatures (considering an inlet velocity of 0.1 m/s) and for all the three cases the conversion linearly increases. At 550 K, the conversion in each reformer was found to be 74.83% in straight annular type, 79.85% in serpentine type, and 82.67% in spiral type. At 600 K, the conversions in all types of reactor were increased and found to be 81.17% in straight annular type, 85.71% in serpentine type, and 87.67% in spiral type. At 650 K, the conversion in the curved channels, increased even more, i.e., 83.66% in straight annular type, 89.17% in serpentine type, and 91.16% in spiral type. Since the reaction is endothermic in nature, the conversion increases with the increase of the temperature. However, upper limit of temperature was fixed at 650–670 K considering the commercial

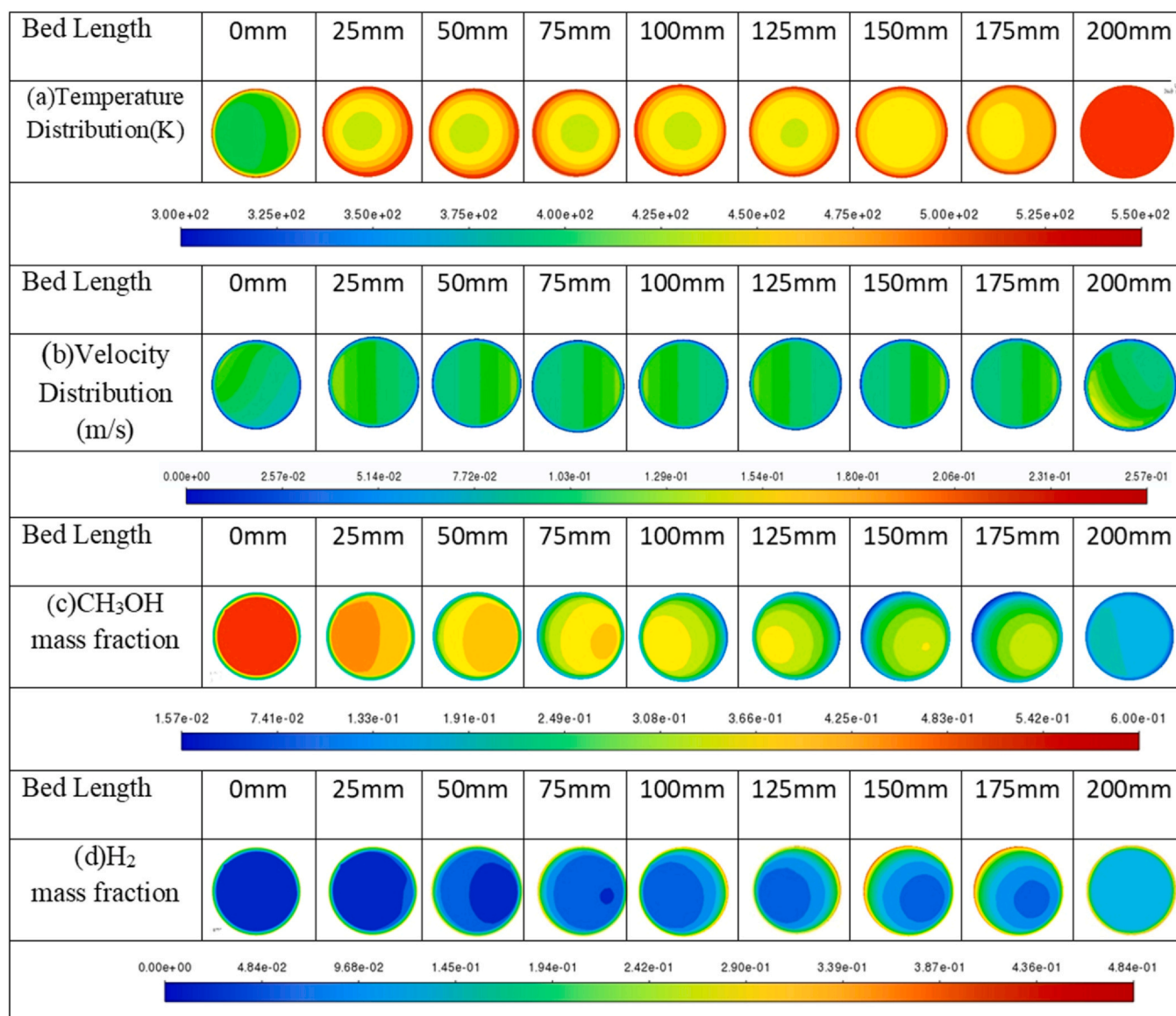


**Fig. 5 – Contour of (a) temperature, (b) velocity and (c) & (d) species distribution along radial cross-sectional planes of the spiral reformer.**

applications of on-board engines. Fig. 7(a) shows the variation of outlet  $H_2$  mass fraction with wall temperature. It was observed that as expected, the  $H_2$  mass fraction increases with the increased wall temperature in all the cases. In the straight annular geometry, the area weighted mass fraction of  $H_2$  at the outlet was 0.069 at 550 K, 0.083 at 600 K, and 0.093 at 650 K. In serpentine geometry, the  $H_2$  production was comparatively better and it was found that the conversions were 0.083, 0.106 and 0.125 at 550 K, 600 K and 650 K respectively. And in spiral geometry, even better production was achieved i.e., 0.098 at 550 K, 0.128 at 600 K, and 0.149 at 650 K. The comparative analysis clearly shows the influence of reformer geometry on the rate of hydrogen production and methanol conversion.

It is interesting to note that the spiral type did not show that much reduction in conversion as well as in  $H_2$  production as the other two types. The  $H_2$  mass fraction at the outlet was also found to be reduced because of the reduction in conversion (Figs. 6(b) and 7(b)). At an inlet velocity of 0.2 m/s, the  $H_2$  mass fraction in straight annular, serpentine and spiral geometry was found to be 0.045, 0.067, and 0.078 respectively. At an inlet velocity of 0.3 m/s, the same was found

to be 0.037, 0.048, and 0.059 respectively. The results indicate that, there was a velocity difference between the inlet and the outlet of the reformer due to the reaction and viscous resistance provided by the porosity of the catalyst material. This velocity difference is more in straight annular, than serpentine and even less in spiral type. Therefore, the velocity has significant influence on conversion rate of the reforming reaction.

In case of spiral type reformer, the residence time inside the catalyst bed region was more and the reformer performance was better. Reforming reaction is also dependent on a parameter called gas hourly space velocity (GHSV), which defines that how long the reactant gas is in contact with the catalyst material inside the reformer. A lower GHSV means that the reactants are in contact with the catalyst longer, increasing methanol conversion and hydrogen yield. (Srivastava et al. 2022). Spiral type reformer exhibits a satisfactory and best reaction performance, as methanol conversion was 3% more than serpentine type and almost 8% more than the straight annular type geometry.

The pressure along the length of the catalyst bed varies depending on the reactor geometry and it has significant



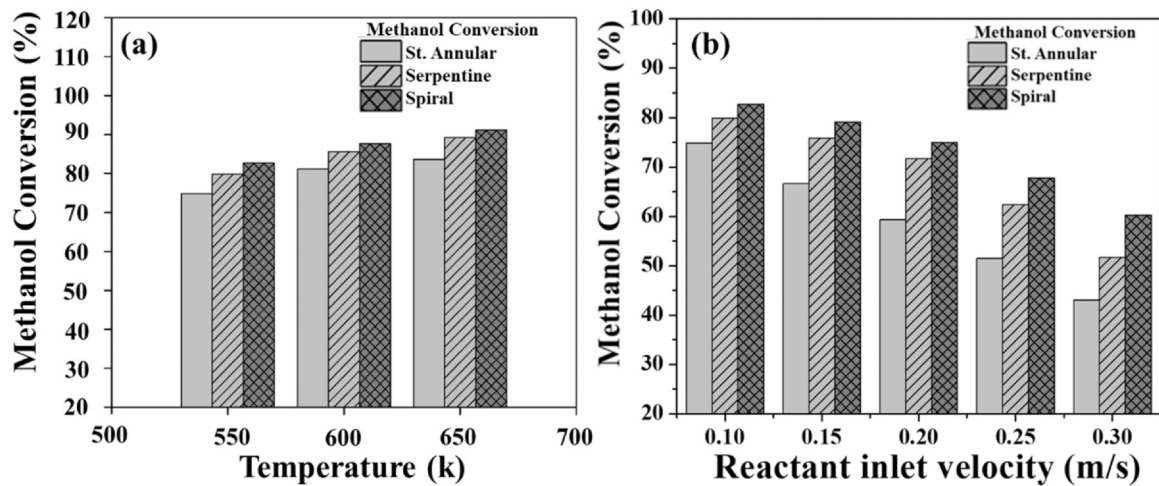


Fig. 6 – Methanol conversion (%) at (a) different wall temperatures and (b) different reactant inlet velocities for different reformer geometries.

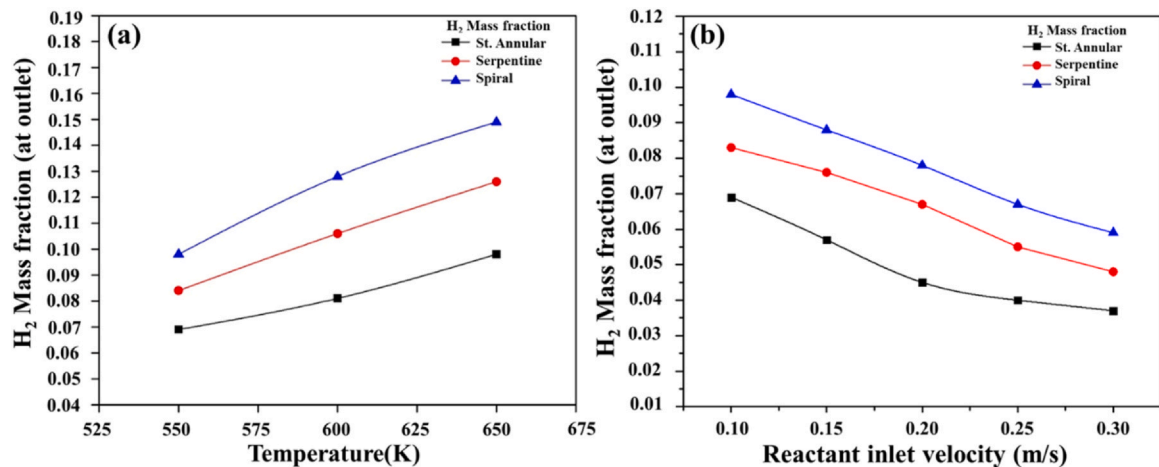


Fig. 7 – Variation of produced  $H_2$  mass fraction (at the outlet) with (a) wall temperatures (K) and (b) reactant inlet velocity (m/s) for different reformer geometry.

influence on the rate of conversion. In order to investigate the effect of pressure on the rate of methanol conversion, the mass fraction of methanol has been calculated along the length of the reactor and plotted in Fig. 8. Variation of the pressure was also shown simultaneously. It has been observed that in all the cases mass fraction of methanol reduces along length of the reactor. In straight annular type (Fig. 8(a)), methanol was converted instantly as soon as it enters the catalyst bed, which is up to 50 mm of bed length. Then the conversion was almost at a fixed rate throughout the rest part of the bed (50–200 mm), and no further conversion was observed. In the serpentine and spiral type (Figs. 8(b) and 8(c)) both the plots were nearly similar. The methanol mass fraction reduced steadily up to 100 mm in both the cases. Though the slope of the methanol mass fraction curve was more in case of spiral type. After that a sudden drop was appeared from 100 mm to 150 mm, which shows that conversion took place more rapidly in that particular region of bed. Finally in spiral type methanol mass fraction was much less than serpentine at the end of the bed. The pressure drop was seen to be slightly more in straight annular, slightly less in serpentine and even lesser in spiral. This was inversely proportional to the velocity drop in each reformer. It was noted how changing the geometry can affect

the pressure drop which make a significant change in the conversion, though the conversion achieved was also depending on other factors like temperature, gas velocity and the geometry. In earlier studies (Pashchenko et al., 2020), it was found that on increasing the pore size of the catalyst bed, pressure drop will decrease. Though the porosity depends on the property of catalyst and in the present study Cu-based catalyst was considered which has a fixed property, it can be proposed that, for different catalyst material, the porosity will be different and the pressure drop will also be depend on that. From the trends of methanol mass fraction, it can be understood that spiral and serpentine types of reformers will be able to produce more hydrogen efficiently than the straight annular type, since methanol was not converting steadily rather after a sudden conversion there was no significant reduction of methanol.

In order to investigate the effect of reactor dimension on the reaction conversion, a number of simulations of the three types of reactors (straight annular, serpentine and spiral) with different diameters were performed keeping the length constant and considering the same initial velocity as 0.1 m/s. The results are presented in Fig. 9. The plot shows a distinct variation of methanol conversion with the variation of the reactor diameter. At a larger diameter of 25 mm, the

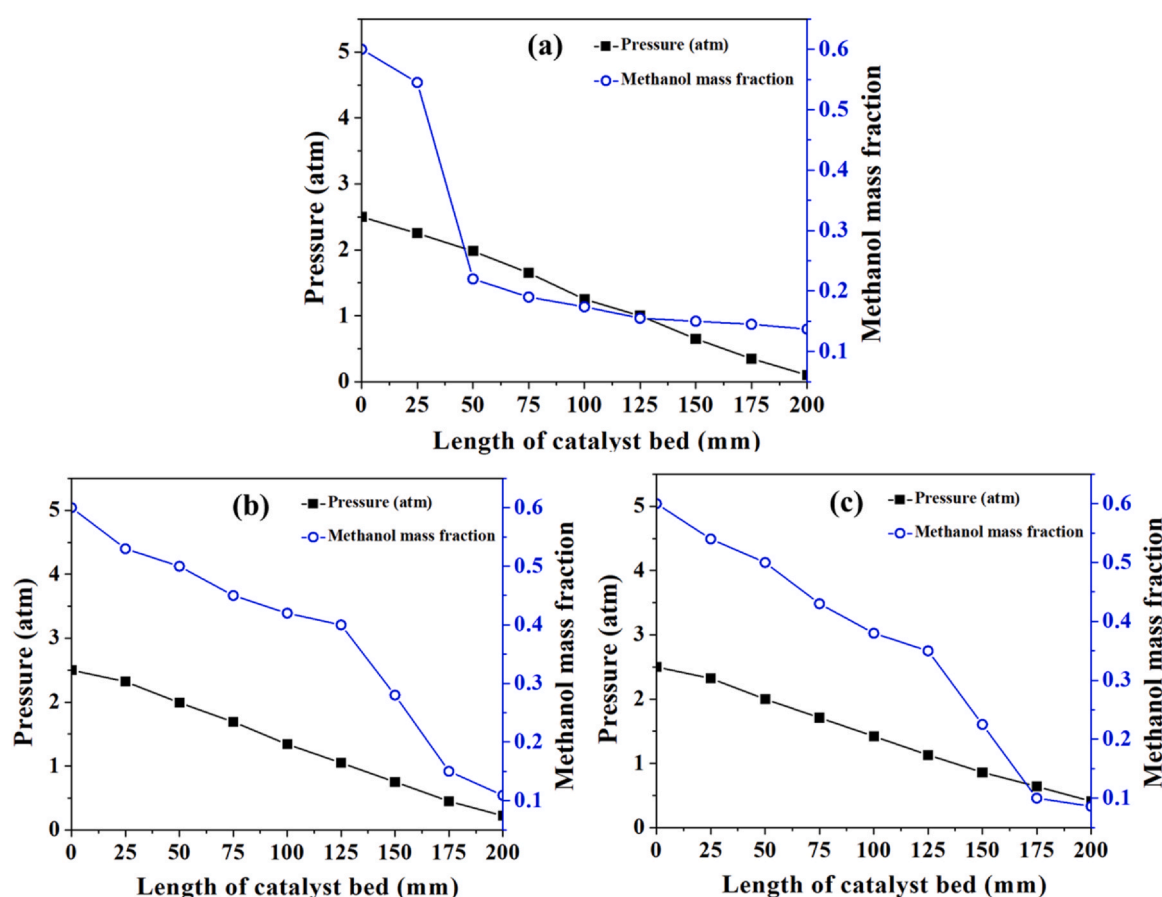


Fig. 8 – Variation of pressure and methanol mass fraction along the length of the catalyst bed; (a) straight annular, (b) serpentine and (c) spiral type.

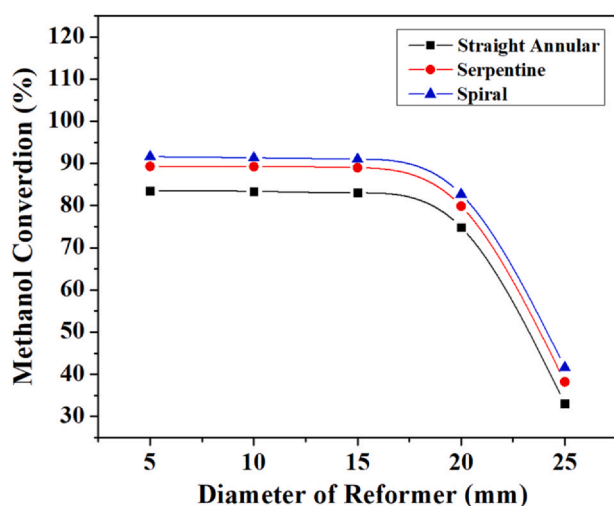


Fig. 9 – Methanol conversion (%) at different reformer diameters for various reformer geometries.

methanol conversion was observed to be significantly low. This decline suggests that larger reactor diameters may not be optimal for achieving high methanol conversion rates. Whereas, at a diameter of 15 mm the conversion was found to be significantly high. It was also observed that decreasing the diameter beyond 15 mm is not showing any change in the methanol conversion. This suggests that the optimal diameter for maximizing conversion lies near 15 mm diameter. This observation implies that the benefits gained from decreasing the diameter beyond a certain point are minimal

or negligible. Therefore, a balance between these factors appears to exist, indicating an optimal diameter range for achieving maximum methanol conversion.

#### 4. Conclusion

A computational fluid dynamics-based analysis on 3-dimensional steam micro-reformers was performed to evaluate the effect of spiral and serpentine type channel geometry packed with Cu based catalyst. Influence of reformer geometry was investigated considering the rate of hydrogen production and methanol conversion. Effect of inlet gas velocity was also analysed. It has been observed from the results that in the spiral and serpentine geometry, the velocity of gas mixture is less than the straight annular type because of the disturbance suffered through the curved channels. GHSV is the reciprocal of space velocity or residence time. GHSV was much lower in spiral reformer than other two reformers which increases the residence time. It was observed that temperature and velocity distribution, which changes based on the reformer geometry, significantly influences the conversion rate. Spiral reformer exhibited conversion up to 91.16% at 650 K and producing 0.15 mass fraction of hydrogen, which was found to be 3% more than the conversion achieved in serpentine type and almost 8% more than the straight annular type geometry when the inlet velocity was kept at 0.1 m/s for all the cases. Similar trend was also observed in case of higher inlet velocities. Hence, the spiral reformer can be chosen as a better design for methanol steam reforming reaction and hydrogen

production. Experimental validation of this prediction is kept as a future scope of research.

## Declaration of Competing Interest

The authors declare that they have no known competing financial interests or personal relationships that could have appeared to influence the work reported in this paper.

## Acknowledgment

We acknowledge the financial support of RIG grant (NIT Durgapur) of AH.

## Appendix A. Supporting information

Supplementary data associated with this article can be found in the online version at [doi:10.1016/j.cherd.2023.06.051](https://doi.org/10.1016/j.cherd.2023.06.051).

## References

- Agrell, Johan, Henrik, Birgersson, Magali, Boutonnet, 2002. Steam reforming of methanol over a Cu/ZnO/Al<sub>2</sub>O<sub>3</sub> catalyst: a kinetic analysis and strategies for suppression of CO formation. *J. Power Sources* 106 (1–2), 249–257. [https://doi.org/10.1016/S0378-7753\(01\)01027-8](https://doi.org/10.1016/S0378-7753(01)01027-8)
- Burke, S.P., Plummer, W.B., 1928. Gas flow through packed columns. *Ind. Eng. Chem.* 20 (11), 1196–1200. <https://doi.org/10.1021/ie50227a025>
- Canonsburg, Technology Drive, 2012. ANSYS FLUENT User's Guide. Knowl. Creat. Diffus. Util. 15317 (October), 724–746.
- Chen, Rei Yu, Chen, Yen Cho, Zhu, Hung Jang, Chung, J.N., 2012. Numerical simulation of flow disturbance and heat transfer effects on the methanol-steam reforming in miniature annulus type reformers. *Energy Fuels* 26 (2), 1202–1213. <https://doi.org/10.1021/ef201498t>
- Chen, Yongping, Zhang, Chengbin, Wu, Rui, Shi, Mingheng, 2011. Methanol steam reforming in microreactor with constructal tree-shaped network. *J. Power Sources* 196 (15), 6366–6373. <https://doi.org/10.1016/j.jpowsour.2011.03.044>
- Chiriac, Radu, Racovitza, Alexandru, Podevin, Pierre, Descombes, Georges, 2015. On the possibility to reduce CO<sub>2</sub> emissions of heat engines fuelled partially with hydrogen produced by waste heat recovery. *Int. J. Hydrog. Energy* 40 (45), 15856–15863. <https://doi.org/10.1016/j.ijhydene.2015.06.064>
- Davda, R.R., Shabaker, J.W., Huber, G.W., Cortright, R.D., Dumesic, J.A., 2003. Aqueous-phase reforming of ethylene glycol on silica-supported metal catalysts. *Appl. Catal. B: Environ.* 43 (1), 13–26. [https://doi.org/10.1016/S0926-3373\(02\)00277-1](https://doi.org/10.1016/S0926-3373(02)00277-1)
- Duc-Khanh Nguyen, Sebastian Verhelst, 2019. Chapter -3, Diluted Combustion of Methanol in Spark-Ignition Engines with On-Board Fuel Reforming, A PhD Thesis.
- Fluent, ANSYS, 2013. MAN - ANSYS Fluent User's Guide Release 15.0. Knowl. Creat. Diffus. Util. 15317 (November), 724–746.
- Fukahori, Shuji, Koga, Hirotaka, Kitaoka, Takuya, Nakamura, Mitsuyoshi, Wariishi, Hiroyuki, 2008. Steam reforming behavior of methanol using paper-structured catalysts: experimental and computational fluid dynamic analysis. *Int. J. Hydrog. Energy* 33 (6), 1661–1670. <https://doi.org/10.1016/j.ijhydene.2007.12.063>
- Gong, Changming, Li, Zhaohui, Sun, Jingzhen, Liu, Fenghua, 2020. Evaluation on combustion and lean-burn limit of a medium compression ratio hydrogen/methanol dual-injection spark-ignition engine under methanol late-injection. *Appl. Energy* 277 (August), 115622. <https://doi.org/10.1016/j.apenergy.2020.115622>
- Gong, Changming, Li, Zhaohui, Yi, Lin, Liu, Fenghua, 2020. Experimental investigation of equivalence ratio effects on combustion and emissions characteristics of an H<sub>2</sub>/methanol dual-injection engine under different spark timings. *Fuel* 262 (October 2019), 116463. <https://doi.org/10.1016/j.fuel.2019.116463>
- Gurau, V., Ogunleke, A., Strickland, F., 2020. Design of a methanol reformer for on-board production of hydrogen as fuel for a 3 KW High-Temperature proton exchange membrane fuel cell power system. *Int. J. Hydrog. Energy* 45 (56), 31745–31759. <https://doi.org/10.1016/j.ijhydene.2020.08.179>
- Hall, J.L., 1987. Cell components. *Phytochemistry* 26 (4), 1235–1236. [https://doi.org/10.1016/S0031-9422\(00\)82398-5](https://doi.org/10.1016/S0031-9422(00)82398-5)
- Hsueh, Ching Yi, Chu, Hsin Sen, Yan, Wei Mon, Leu, Guang Ching, Tsai, Jong Ian, 2011. Three-dimensional analysis of a plate methanol steam micro-reformer and a methanol catalytic combustor with different flow channel designs. *Int. J. Hydrog. Energy* 36 (21), 13575–13586. <https://doi.org/10.1016/j.ijhydene.2011.07.099>
- Iulianelli, A., Ribeiro, P., Mendes, A., Basile, A., 2014. Methanol steam reforming for hydrogen generation via conventional and membrane reactors: a review. *Renew. Sustain. Energy Rev.* 29, 355–368. <https://doi.org/10.1016/j.rser.2013.08.032>
- Karim, Ayman, Bravo, Jaime, Datye, Abhaya, 2005. Nonisothermality in packed bed reactors for steam reforming of methanol. *Appl. Catal. A: Gen.* 282 (1–2), 101–109. <https://doi.org/10.1016/j.apcata.2004.12.006>
- Karim, Ayman, Bravo, Jaime, Gorm, David, Conant, Travis, Datye, Abhaya, 2005. Comparison of wall-coated and packed-bed reactors for steam reforming of methanol. *Catal. Today* 110 (1–2), 86–91. <https://doi.org/10.1016/j.cattod.2005.09.010>
- Kim, Taegyu, 2009. Micro methanol reformer combined with a catalytic combustor for a PEM fuel cell. *Int. J. Hydrog. Energy* 34 (16), 6790–6798. <https://doi.org/10.1016/j.ijhydene.2009.06.024>
- Kreuer, K.D., 2001. On the development of proton conducting polymer membranes for hydrogen and methanol fuel cells. *J. Membr. Sci.* 185 (1), 29–39. [https://doi.org/10.1016/S0376-7388\(00\)00632-3](https://doi.org/10.1016/S0376-7388(00)00632-3)
- Luo, Qing he, Hu, Ji. Bin, Sun, Bai gang, Liu, Fu. shui, Wang, Xi, Li, Chao, Bao, Ling zhi, 2019. Experimental investigation of combustion characteristics and NO<sub>x</sub> emission of a turbo-charged hydrogen internal combustion engine. *Int. J. Hydrog. Energy* 44 (11), 5573–5584. <https://doi.org/10.1016/j.ijhydene.2018.08.184>
- Mathur, S., Saxena, S.K., 1965. Viscosity of polar gas mixtures: Wilke's method. *Appl. Sci. Res.* 15 (1), 404–410. <https://doi.org/10.1007/bf00411574>
- Meille, V. 2021. "Review on Methods to Deposit Catalysts on Structured Surfaces To Cite This Version: HAL Id: Hal-00115981 Review on Methods to Deposit Catalysts on Structured Surfaces."
- Nehe, Prashant, Mahendra Reddy, V., Kumar, Sudarshan, 2015. Investigations on a new internally-heated tubular packed-bed methanol-steam reformer. *Int. J. Hydrog. Energy* 40 (16), 5715–5725. <https://doi.org/10.1016/j.ijhydene.2015.02.114>
- Niu, Renxu, Yu, Xiumin, Du, Yaodong, Xie, Hanguang, Wu, Haiming, Sun, Yao, 2016. Effect of hydrogen proportion on lean burn performance of a dual fuel SI engine using hydrogen direct-injection. *Fuel* 186, 792–799. <https://doi.org/10.1016/j.fuel.2016.09.021>
- Pashchenko, Dmitry, 2020. How to choose endothermic process for thermochemical waste-heat recuperation? *Int. J. Hydrog. Energy* 45 (38), 18772–18781. <https://doi.org/10.1016/j.ijhydene.2020.04.279>
- Pashchenko, Dmitry, 2021. Thermochemical waste-heat recuperation as on-board hydrogen production technology. *Int. J. Hydrog. Energy* 46 (57), 28961–28968. <https://doi.org/10.1016/j.ijhydene.2020.11.108>
- Pashchenko, Dmitry, Karpilov, Igor, Mustafin, Ravil, 2020. Numerical calculation with experimental validation of pressure drop in a fixed-bed reactor filled with the porous elements. *AIChE J.* 66 (5), 1–9. <https://doi.org/10.1002/aic.16937>
- Peppley, Brant A., Amphlett, John C., Kearns, Lyn M., Mann, Ronald F., 1999. Methanol-steam reforming on Cu/ZnO/Al<sub>2</sub>O<sub>3</sub> catalysts. Part 2. A comprehensive kinetic model. *Appl. Catal.*

- A: Gen. 179 (1–2), 31–49. [https://doi.org/10.1016/S0926-860X\(98\)00299-3](https://doi.org/10.1016/S0926-860X(98)00299-3)
- Perng, Shiang Wu, Horng, Rong Fang, Wu, Horng Wen, 2017. Effect of a diffuser on performance enhancement of a cylindrical methanol steam reformer by computational fluid dynamic analysis. *Appl. Energy* 206 (August), 312–328. <https://doi.org/10.1016/j.apenergy.2017.08.194>
- Srivastava, Alankrit, Kumar, Parmod, Dhar, Atul, 2022. Performance enhancement of methanol reforming reactor through finned surfaces and diffused entry for on-board hydrogen generation. *Int. J. Hydrog. Energy* 47 (11), 7478–7490. <https://doi.org/10.1016/j.ijhydene.2021.12.084>
- Sun, Yao, Yu, Xiumin, Jiang, Linlin, 2016. Effects of direct hydrogen injection on particle number emissions from a lean burn gasoline engine. *Int. J. Hydrog. Energy* 41 (41), 18631–18640. <https://doi.org/10.1016/j.ijhydene.2016.07.224>
- Tadbir, M.Andisheh, Akbari, M.H., 2011. Methanol steam reforming in a planar wash coated microreactor integrated with a micro-combustor. *Int. J. Hydrog. Energy* 36 (20), 12822–12832. <https://doi.org/10.1016/j.ijhydene.2011.05.010>
- Taylor, Publisher, J.P. Van Doormaal, and G.D. Raithby. 2007. “Numerical Heat Transfer: An International Journal of Computation and Methodology enhancements of the simple method for predicting incompressible fluid flows (February 2013):37–41.
- Vadlamudi, Vinay K., Palanki, Srinivas, 2011. Modeling and analysis of miniaturized methanol reformer for fuel cell powered mobile applications. *Int. J. Hydrog. Energy* 36 (5), 3364–3370. <https://doi.org/10.1016/j.ijhydene.2010.12.062>
- White, F.M. (1991). *Viscous Fluid Flow*. McGraw-Hill Science, Engineering & Mathematics.
- Zhang, Shubin, Zhang, Yufeng, Chen, Junyu, Zhang, Xuelin, Liu, Xiaowei, 2017. High yields of hydrogen production from methanol steam reforming with a cross-U type reactor. *PLoS ONE* 12 (11), 1–14. <https://doi.org/10.1371/journal.pone.0187802>
- Zhuang, Xiaoru, Xu, Xinhai, Li, Lun, Deng, Daxiang, 2020. Numerical investigation of a multichannel reactor for syngas production by methanol steam reforming at various operating conditions. *Int. J. Hydrog. Energy* 45 (29), 14790–14805. <https://doi.org/10.1016/j.ijhydene.2020.03.207>